Journal of Materials and Environmental Science
ISSN : 2028-2508
e-ISSN : 2737-890X
CODEN : JMESCN

J. Mater. Environ. Sci., 2024, Volume 15, Issue 9, Page 1331-1346

http://www.jmaterenvironsci.com

Role of NDVI in Assessing Surface Urban Heat Island phenomenon: A Case Study of Alappuzha District, Kerala

Anitha V. [1], Prabha D. [1*]

[1]*Department of Environmental Sciences, Bharathiar University, Coimbatore - 641046, Tamil Nadu, India*
**Corresponding author, Email address: prabha.ens@buc.edu.in*

Received *23 Sept 2024,*
Revised *26 Sept 2024,*
Accepted *27 Sept 2024*

Keywords:

- ✓ *Normalized Difference Vegetation Index;*
- ✓ *Land Surface Temperature;*
- ✓ *Surface Urban Heat Island;*
- ✓ *Landsat OLI and TIRS;*
- ✓ *Landsat TM*

Citation*: Anitha V., Prabha D. (2024) Role of NDVI in Assessing Surface Urban Heat Island phenomenon: A Case Study of Alappuzha District, Kerala, J. Mater. Environ. Sci., 15(9), 1331-1346*

Abstract: The present study involved analyzing the impact of Normalized Difference Vegetation Index (NDVI), a measure of vegetation density, on Land Surface Temperature (LST) and its role in the formation of Surface Urban Heat Island (SUHI) effect in Alappuzha district, Kerala. Imagery from Landsat TM, Landsat OLI and TIRS for the years 1988 and 2020 was utilized to evaluate the correlation between NDVI and SUHI. The land area corresponding to each NDVI category were quantified. The results revealed that NDVI of the study area declined from 1 in 1988 to 0.56 in 2020, resulting in an increase in maximum and mean LST. LST_{Max} increased from 32.98°C in 1988 to 37.44°C in 2020. LST_{Mean} which was 25.66°C in 1988 increased to 26.88°C in 2020. The decrease in NDVI led to a rise in the high SUHI classes such as Middle, Strong and Stronger by 128.62%, 47.66% and 47.66% respectively. A negative correlation was observed between NDVI and LST, with Pearson coefficients of – 0.4874 for 1988 and – 0.4097 for 2020, indicating that NDVI might be utilized as an important indicator to analyze LST and SUHI effects.

1. Introduction

The rapid urbanization of any region often brings about significant changes in their Land Use and Land Cover (LULC) patterns, resulting in the conversion of natural landscapes into artificial surfaces and impervious structures (Kuang *et al.*, 2019). This transformation contributes to the increase in Land Surface Temperature (LST) by enhancing the absorption of solar radiation and reducing the loss of long-wave radiation, which ultimately affects local climatic conditions (Faqe Ibrahim *et al.*, 2017). Increase in impervious surfaces elevates surface temperatures resulting in genesis of Urban Heat Island (UHI) effects (Carpio *et al.*, 2020), wherein urban areas tend to have warmer temperatures than their rural counterparts (Carpio *et al.*, 2020; Hussain *et al.*, 2022). The reduction in vegetative cover due to urban sprawl further exacerbates this effect by diminishing the cooling effects provided by green spaces through shade and evapotranspiration (Xiong *et al.*, 2012; Chkird *et al.*, 2024).

Research into UHI effects often involves analyzing LST variations, which reflect the different thermal responses of various land covers (Streutker, 2003). Remote sensing technology has proven effective in these studies, allowing for detailed assessments of LST and its correlation with land

cover changes (Zhou *et al.*, 2013; Siddique *et al.*, 2020). Vegetation indices such as the Normalized Difference Vegetation Index (NDVI) are commonly used to evaluate changes in vegetation cover, which can indicate shifts in LULC and their impact on LST (Lo and Quattrochi, 2003).

Several studies have explored the relationship between LULC changes, LST, and UHI across various global cities. For example, Julien *et al.* (2011) examined temporal analysis of NDVI on LST in Iberia, while Mallick *et al.* (2008) and Dutta *et al.* (2021) focused on LST variations in Delhi. Impact of Land cover changes on LST in Bangalore (Santhosh and Shilppa, 2023) and impact of Land cover indices on LST in Ahmedabad (Mathew *et al.*, 2022) and Surat (Vasanthawada *et al.,* 2022) have been reported. Significant correlations between Urban expansion and increased surface temperatures have also been reported for Chennai (Amirtham *et al.*, 2009), Jaipur (Chandra *et al.*, 2018) Pune (Gohain *et al.*, 2021) and Raipur (Guha *et al.*, 2022).

Global research on Urban Heat Island (UHI) dynamics frequently employs Landsat imagery and remote sensing indices. The link between LST and vegetation for UHI analysis have been examined in Indianapolis, (Weng *et al.*, 2004), Wuhan (Zhang *et al.*, 2012), Skopje (Kaplan *et al.*, 2018) and in Mekelle City (Tesfamariam *et al.*, 2023). In India, Grover and Singh (2015) analyzed NDVI and UHI in Delhi and Mumbai. Aggarwal and Misra (2018) found NDBI to be a better SUHI intensity indicator than NDVI in Bangalore and New Delhi. Increased surface temperature associated with urbanization, negatively impacting vegetation has been reported by Mathew *et al.* (2017) for Jaipur. Bora and Bora (2023) analyzed LULC changes in Charaideu district, Assam, using NDVI and Normalized Difference Moisture Index (NDMI).

In Kerala, there is a lack of information depicting the relationship between NDVI and LST, particularly in Alappuzha district. While some research has been conducted in neighboring regions like Ernakulam (Radhakrishnan and Geetha, 2022), Kottayam (Anitha *et al.*, 2023) and Kollam (Mathew and Varghese, 2022), the specifics of Alappuzha's LULC changes and their impacts on LST and SUHI remain underexplored. Therefore, this study aims to fill this gap by analyzing the effects of NDVI on SUHI phenomena in Alappuzha district from 1988 to 2020, employing advanced geospatial techniques to provide a detailed understanding of these dynamics.

2. Methodology

2.1 Study Area

Alappuzha (**Figure 1**), a smallest district in Kerala, is situated between latitudes 9° 06' 36" and 9° 53' 30" N and longitudes 76° 19' 03" and 76° 41' 33" E longitudes. Bordered by Ernakulam to the north, Kottayam and Pathanamthitta to the east, the Lakshadweep Sea to the west, and Kollam to the south, it spans 1,414 Km^2. The 2011 census reported a population of 2,127,789, with a density of 1,504 people per square kilometer. The district features a sandy landscape with lagoons, rivers, and canals, and lacks significant elevations except for some hillocks in the eastern parts between Bharanikkavu and Chengannur. The Ambalappu, Cherthala, Karthikappally, and Kuttanad Taluks are located in lowland areas. Approximately 80% of the district is coastal, with a coastline of 82 kilometers, while the remaining 20% is midland. Alappuzha is unique in Kerala for having no high land or forested areas, with waterbodies covering 13% of the district and much of the area below sea level. The climate is hot and moist along the coast and slightly cooler and drier inland, with an average temperature of 25°C and annual rainfall of 2,763 mm.

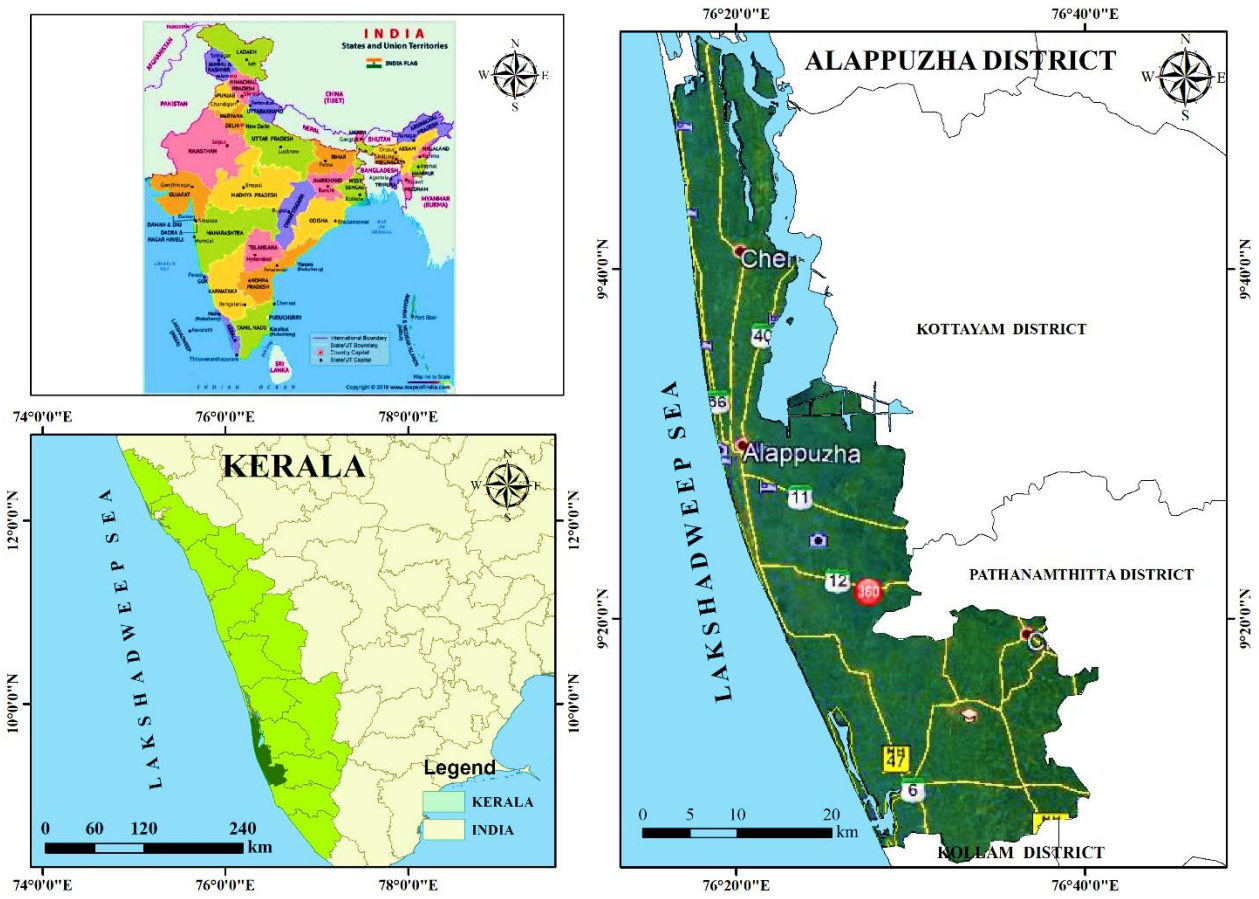

Figure 1. Map of the study area

2.2. Data Acquisition

In this study, Four Landsat images (path/row: 144/53 and 144/54) were obtained from the United States Geological Survey (USGS) website (https://earthexlorer.usgs.gov/) for two different years. Landsat 5 TM (1988) and Landsat 8 OLI/TIRS (2020) were based on the remark of minimum cloud cover and of the same month (January) to achieve marginal atmospheric and seasonal effects (Emran *et al.,* 2018). **Table 1** presents a description of the three Landsat datasets utilized in the study.

Table 1. Characteristics of Landsat images used for the study.

Satellite	Sensor	Path/Row	Date of Image Acquisition	Spatial Resolution	Cloud Cover
Landsat -5	Thematic Mapper (TM)	144/53	19/01/1988	30	9
		144/54			6
Landsat -8	Operational Land Imager (OLI) and Thermal Infrared	144/53	27/01/2020	30	0.78
		144/54			14.30

2.3. Image Mosaicking

The study area spanned two image rows (53 and 54). Mosaicking was performed to merge these into a single raster image, which involved dealing with overlapping areas where Digital Number (DN) values varied. The 'Maximum' Mosaic Method was chosen to assign the highest value to overlapping areas, avoiding '0' values. Additionally, the 'Match' Mosaic Colour Mode was used to ensure consistent color mapping during the process.

2.4. Retrieval of LST

Satellite image data is stored as a Digital Number (DN), which provide an indirect representation of the spectral radiances from objects on the ground. To calculate LST, images from Landsat 5 (band 6) and Landsat 8 (band 10) are utilized. Even though Landsat 8 has two thermal bands (bands 10 and 11), band 11 is not used according to USGS recommendation, due to the high calibration uncertainty. As a result, only band 10 is used in this study's LST calculation (Ihlen, 2019; Barsi *et al.,* 2014). The process of deriving LST from Landsat TM and Landsat OLI involves slight differences in the calculation of spectral radiance (L_λ).

2.4.1. Conversion of DN to L_λ

The first step in LST retrieval is to convert the digital number (DN) of ground objects to spectral radiance using equation 1 in the TIRS sensor (Ihlen, 2019; Landsat 7 Data Users Handbook Used for Landsat 5). The calculation of L_λ from thermal bands of Landsat TM/ETM+ and OLI/TIRS is carried out using the equation provided below.

For Landsat 5,

$$L_\lambda = \frac{\left(L_{MAX_\lambda} - L_{MIN}\right)}{\left(Q_{Cal_{MAX}} - Q_{Cal_{MIN}}\right)} \times \left(Q_{Cal} - Q_{Cal_{MIN}}\right) + L_{MIN} \qquad \textbf{Eqn. 1}$$

In the above equation, L_λ represents Spectral Radiance, L_{MAX_λ} corresponds to maximum spectral radiance (15.303 for TM and 17.04 for ETM+), L_{MIN} signifies for the minimum spectral radiances (1.238 for TM), $Q_{Cal_{MAX}}$ stands for the maximum Digital Number (DN) Value (255), $Q_{Cal_{MIN}}$ denotes the minimum DN value (1), Q_{Cal} represents the DN of band 6.

The values for L_{MAX}, L_{MIN}, $Q_{Cal_{MAX}}$ and $Q_{Cal_{MIN}}$ were obtained from metadata file associated with Landsat images. For Landsat 8 OLI thermal band, top of atmospheric radiance (L_λ) was computed using the method described below (Chander and Markham, 2003).

For Landsat 8,

$$L_\lambda = M_L * Q_{cal} + A_L \qquad \textbf{Eqn. 2}$$

Where, M_L denotes the multiplicative rescaling factor specific to the band, with a value = 0.0003342; Q_{cal} represent the DN corresponding to band 10; A_L indicates the additive rescaling factor for the band, which is 0.1.

Conversion of L_λ to TB (At-satellite brightness temperature): The TB from spectral radiance was derived from the following equation (**Eqn. 3**)

$$TB = \frac{K_2}{\ln\left[\frac{K_1}{L_\lambda}+1\right]} \qquad \textbf{Eqn. 3}$$

TB denotes the satellite brightness temperature measured in Kelvin (K), while K_1 and K_2 refer to the calibration constants unique to the TM and OLI & TIRS Sensors, respectively. The values of K_1 and K_2 were 607.76 and 1260.56 for Landsat 5TM, 666.09 and 1287.71 and 1321.0789 for Landsat 8 OLI, respectively (Landsat 5 obtained from Landsat 7 Data Users Handbook 2019; Landsat 8 Data Users Handbook 2019).

Kelvin (K) to Celsius (^{0}C) degrees

$$TB = \frac{K_2}{\ln\left[\frac{K_1}{L_\lambda}+1\right]} - 273.15 \qquad \textbf{Eqn. 4}$$

2.4.2. LST Calculation

The obtained temperature values, known as black body temperatures, were adjusted for spectral emissivity (Ɛ) to derive the LST. The Emissivity correction was performed based on the type of land cover, utilizing NDVI values for each pixel, as outlined by Snyder *et al.* (1988). The corrected LST was then calculated following the method described by Artis and Carnahan (1982).

$$LST = \left[\frac{TB}{1+(\lambda * TB/\rho)*\ln(\varepsilon)}\right] \quad \textbf{Eqn. 5}$$

Where, LST expressed in degrees Celsius (°C). The symbol λ represents the wavelength of the emitted radiance in meters, with a value of 11.45 meters for Landsat 5 (Band 6)) and 10.8 meters for Landsat 8 (Band 10).

$$\boldsymbol{\rho} = h*c/s = 1.4388*10^{-2}\ m\ K \quad \textbf{Eqn. 6}$$

K represents constant with a value of 14388μm K, h denotes Planck's constant, which has a value $6.626*10^{-34}$ J s. The s refers to the Boltzmann constant, value at $1.38 * 10^{-23}$ J/K. Lastly, c represents the velocity of light, approximately $2.998*10^{8}$ m/s.

$$\text{Land surface emissivity } (\varepsilon) = 0.004*P_V+0.986 \quad \textbf{Eqn. 7}$$

Apply the equation in the raster calculator, the value of 0.986 corresponds to a correction value of the equation.

Where the Proportion of vegetation (P_V) can be calculated as;

$$P_V = \text{Square}\ ((NDVI - NDVI_{Min}) / (NDVI_{Max} - NDVI_{Min}) \quad \textbf{Eqn. 8}$$

Generally, the $NDVI_{Minimum}$ and $NDVI_{Maximum}$ values can be directly conveyed through the image. NDVI can be calculated as:

$$NDVI = \text{Float}\ (NIR\text{-}RED)/\text{Float}\ (NIR+RED) \quad \textbf{Eqn. 9}$$

For Landsat 5 Float (4-3)/ Float (4+3)

For Landsat 8, Float (5-4)/ Float (5+4).

2.5. Estimation of NDVI

The NDVI is commonly utilized for assessing vegetation. It is calculated by taking the difference between near-infrared and red reflectance and dividing it by their sum, which provides insights into vegetation phenology (Dissanayake *et al.*, 2019). The extraction of NDVI follows the method outlined by Tucker (1979) and further developed by Townshend and Justice (1986). NDVI value ranges from -1 to 1, where negative values typically indicate the presence of water, while positive values signify vegetation. High values correspond to area with dense vegetation.

$$NDVI = \frac{NIR-Red}{(NIR+Red)} \quad \textbf{Eqn. 10}$$

2.6. Mapping of Surface Urban Heat Island (SUHI)

The urban heat island (SUHI) is identified from the LST range value by **Eqn. 11** (Ullah *et al.*, 2022).

$$SUHI = \frac{T-T_{min}}{T_{min}} \quad \textbf{Eqn. 11}$$

T is the LST raster value, and T_{min} is the minimum LST value of the study area.

3. Results and Discussion

3.1 Analysis of LST

Figure 2a and b shows the spatiotemporal dynamics of LST in Alappuzha from 1988 to 2020. The results show fluctuations in overall LST for the study period. In 1988, the LST_{Min} was 21.61°C,

the LST_{Max} was 32.98°C, and the LST_{Mean} was 25.66°C. The LST_{Min} and LST_{Max} in 2020 were 17.46 and 37.44°C, respectively, with a mean of 26.88. The spatio-temporal dynamics of LST categories in Alappuzha from 1988 to 2020 is illustrated in **Figure 2c** and **Table 2**.

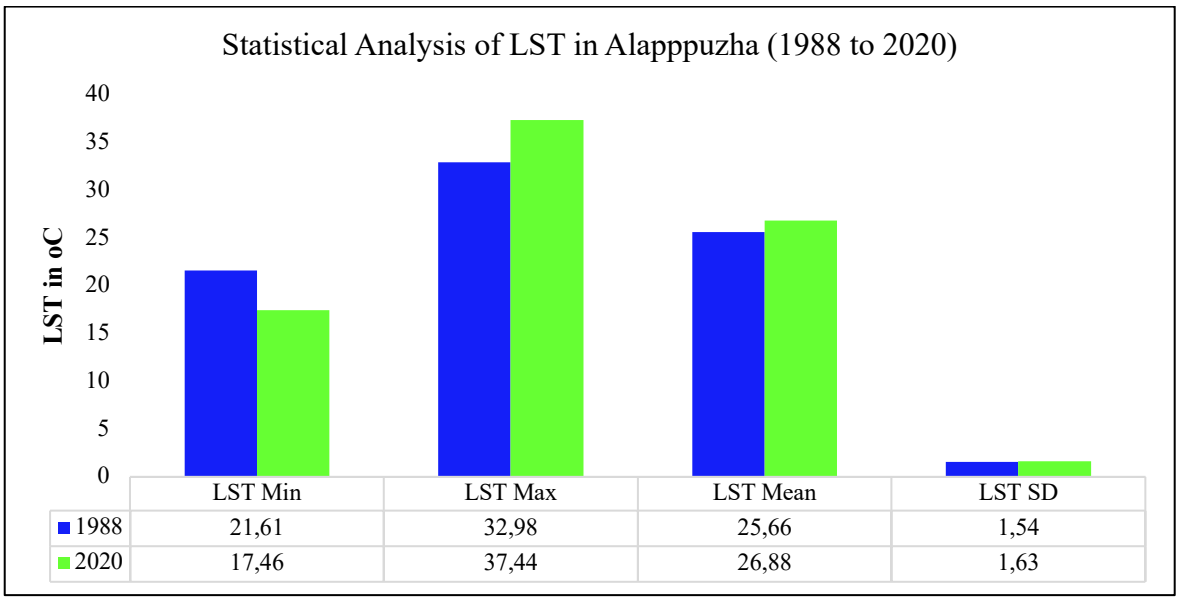

	LST Min	LST Max	LST Mean	LST SD
1988	21,61	32,98	25,66	1,54
2020	17,46	37,44	26,88	1,63

Figure 2a. Statistical Analysis of LST (°C) of Alappuzha District

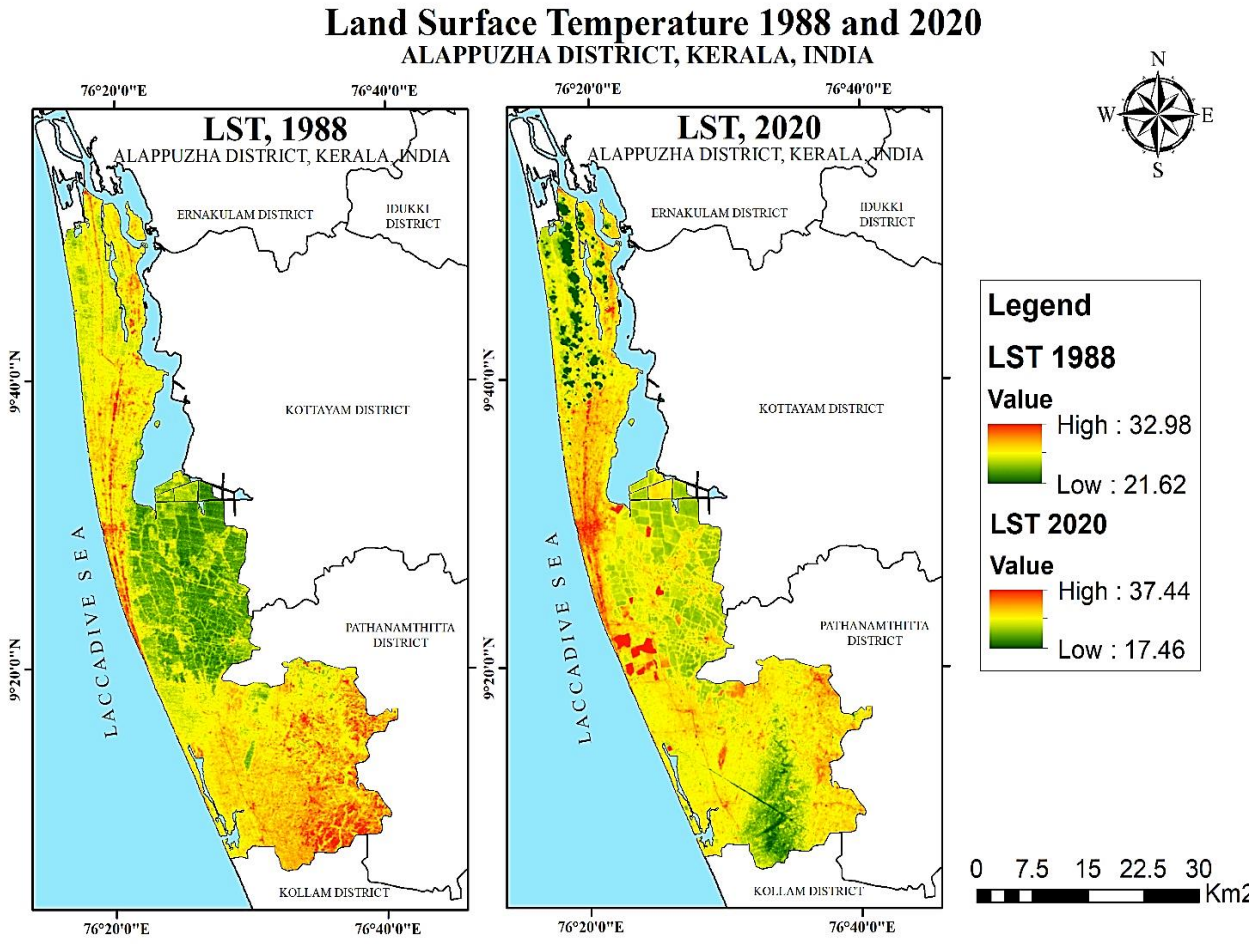

Figure 2b. Spatial distribution of LST (°C) range of Alappuzha District

Table 2. Spatial distribution of LST (ºC) class of Alappuzha District from 1988 to 2020

LST (ºC) Categories	LST Classes	Area km^2 (Area in %)		% Difference (1988 to 2020)
		1988	**2020**	
< 20	Very low	0	7.63	--
20 – 25	Low	403.02 (32.37)	84.84 (6.81)	- 78.95
25 – 30	Medium	837.12 (67.23)	1125.53 (90.40)	34.45
30 – 35	High	4.96 (0.40)	26.31 (2.11)	430.29
>35	Very high	0	0.79 (0.06)	--

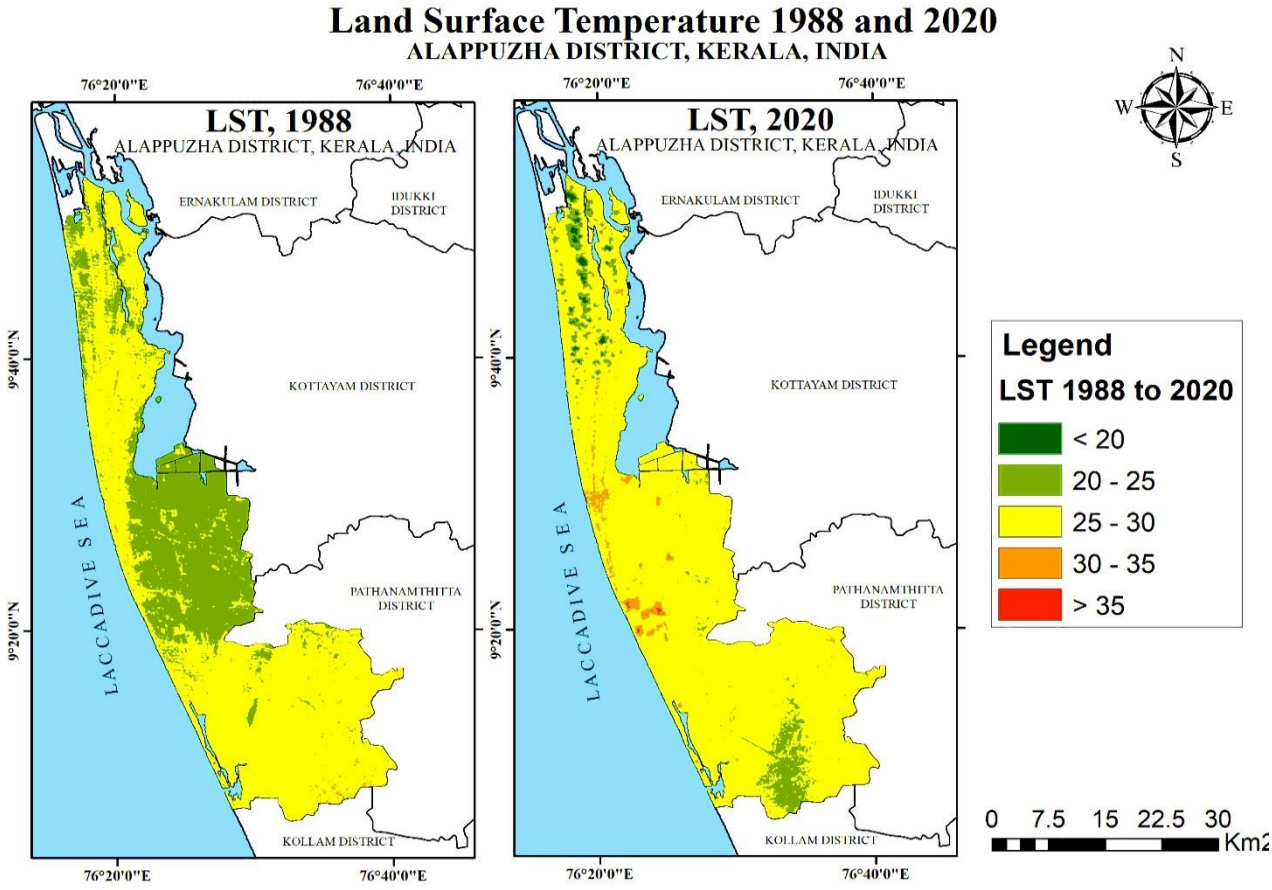

Figure 2c. Spatial distribution of LST (ºC) classes of Alappuzha District

LST was categorized into five classes based on temperature range which were (i) very low (<20 ºC), (ii) low (20-25 ºC), (iii) medium (25-30 ºC), (iv) high (30-35 ºC), and (v) very high (>35 ºC). In 1988, there was no area under the very low LST category. By 2020, 7.63 km^2 (0.61%) was included under this category. The area under low LST which was 403.02 km^2 in 1988 decreased to 84.84 km^2 in 2020, recording a decrease of 78.95%. Area under medium LST increased from 837.12 in 1988 to 1125.53 in 2020, with 34.45% increase. Area under high category in 1988 was 4.96 km^2, which

increased to 26.31 km^2, with a 430.29% growth. The very high LST category was observed only in 2020 with an area of 0.79 km^2 (0.06%), which was not prevalent in 1988.

The results of the LST analysis is suggestive of the fact that LST variations could be due to transformations of LULC, which evolve as the areas become urbanized. In 1988, Alappuzha had high agricultural areas, vegetative cover and water bodies, hence LST was also less. Over the 32 year study period from 1988 to 2020, the maximum temperature increased by 4.46^{o}C reaching 37.44 ^{o}C. This increase in LST may be attributed to developmental activities, especially built-up areas and infrastructure development. The population in the study area grew from 1,865,580 in 1981 to 2,127,789 by 2011, leading to increased demand for residential, commercial, and infrastructural development, contributing significantly to the expansion of built-up land, as has been reported by Prasad and Ramesh (2019) subsequently resulting in increase in LST. Reduction in vegetative cover and water bodies also contribute to increase in the LST_{Max} by 4.46^{o}C and LST_{Mean} 1.22^{o}C thereby contributing to the expansion of Medium and High LST zones. Our results corroborate with the findings of Radhakrishnan and Geetha (2022) who demonstrated increase in LST owing to LULC changes in Kerala's Ernakulam district, showing increase in built-up area by 2% and decline of water bodies and wetlands by 1%. The absence of high dense vegetation cover in 2020 (**Table 3**) would have contributed to the generation of very high LST in the Alappuzha region. Rapid expansion of urban and/or built-up areas along with impervious materials such as materials used for construction and other infrastructure developments are reported as key factors for increase in urban temperatures (Guo *et al.,* 2019). The flourishing tourism industry in Alappuzha is another significant driver of the increase in built-up area. Tourism, apart from imparting economic benefits to local communities, also exerts stress on natural resources and ecosystems. The development of resorts, hotels, restaurants and other infrastructures has contributed to the degradation and habitat fragmentation in certain areas of the region, further accelerating the expansion of built-up land.

3.2 Analysis of NDVI

The statistical analysis and spatial distribution of NDVI range for the years 1988 to 2020 is depicted in **Figures 3a and b** respectively. NDVI values for Alappuzha from 1988 to 2020 indicate fluctuations in vegetation health and density over the years. The minimum and maximum NDVI values ranged from -0.41 to 1 in 1988 and -0.13 to 0.56 in 2020. The maximum NDVI was 1 in 1988, which decreased to 0.56 in 2020, indicating low vegetation density in 2020, compared to 1988. This is evident from our results (**Table 3**) where major changes were effected in the vegetative classes in Alappuzha.

The spatial distribution of NDVI classification for the years 1988 to 2020 is depicted in **Figure 3c** and **Table 3**. In 1988, areas with no vegetation (<0) covered 41.86 km^2 (3.36%), which decreased to 25.60 km^2 (2.06%) in 2020, with 38.85% drop. Very Low vegetation cover was 150.13 km^2 (12.06%) in 1988 which increased to 277.31 km^2 (22.27%) in 2020, with 84.71% growth. Sparse vegetation witnessed substantial growth from 508.09 km^2 (40.81%) in 1988 to 885.46 km^2 (71.12%) in 2020. Moderate vegetation decreased from 442.01 km^2 (35.50%) in 1988 to 56.74 km^2 (4.56%) in 2020. The area covered by highly dense vegetation (>0.60) in 1988 was 103.02 km^2 (8.27%) and there is no highly dense vegetative cover in 2020. Reduction in green cover results in decreased evaporative cooling, thereby causing a rise in LST, as observed in our study.

LULC changes are closely associated with population growth and urbanization. Prasad and Ramesh (2019) reported an increase in the built-up area in Alappuzha from 1973 to 2017. The

growing culture of nuclear families has also contributed to the expansion of built-up areas and the reduction of vegetative cover. The shift of families toward education and non-agricultural employment has reduced the agricultural workforce, resulting in abandoned or repurposed farmland. The appeal of jobs in the secondary sector and rising literacy rates have also made agriculture less attractive (Firoz *et al.*, 2014), further decreasing the extent of agricultural land and green cover and increasing built-up areas.

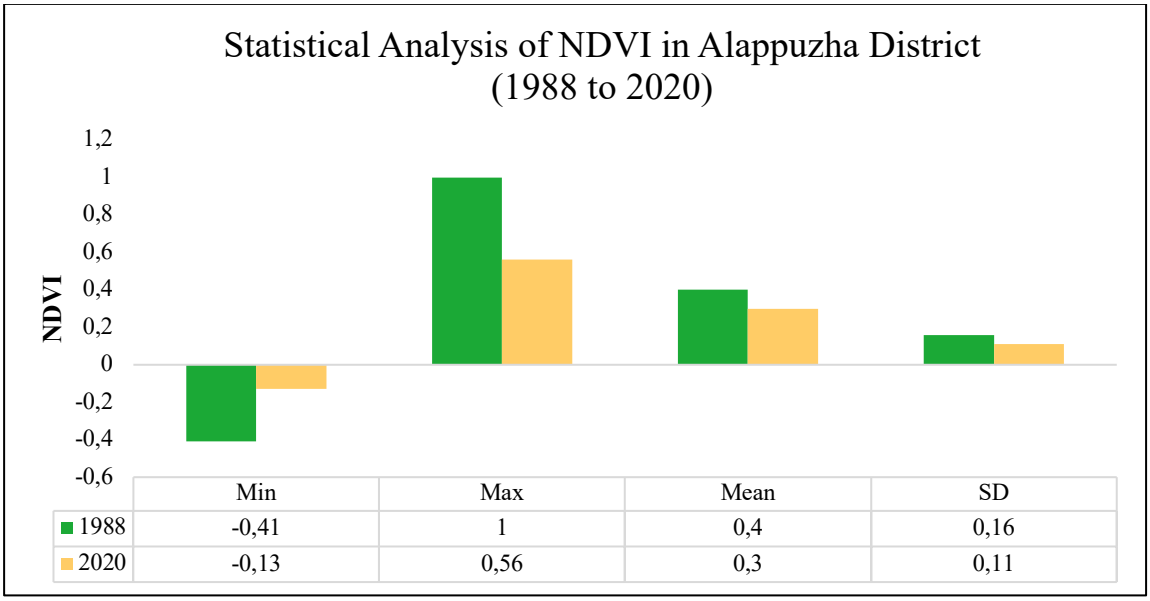

	Min	Max	Mean	SD
1988	-0,41	1	0,4	0,16
2020	-0,13	0,56	0,3	0,11

Figure 3a. Spatial distribution of NDVI range of Alappuzha from 1988 to 2020

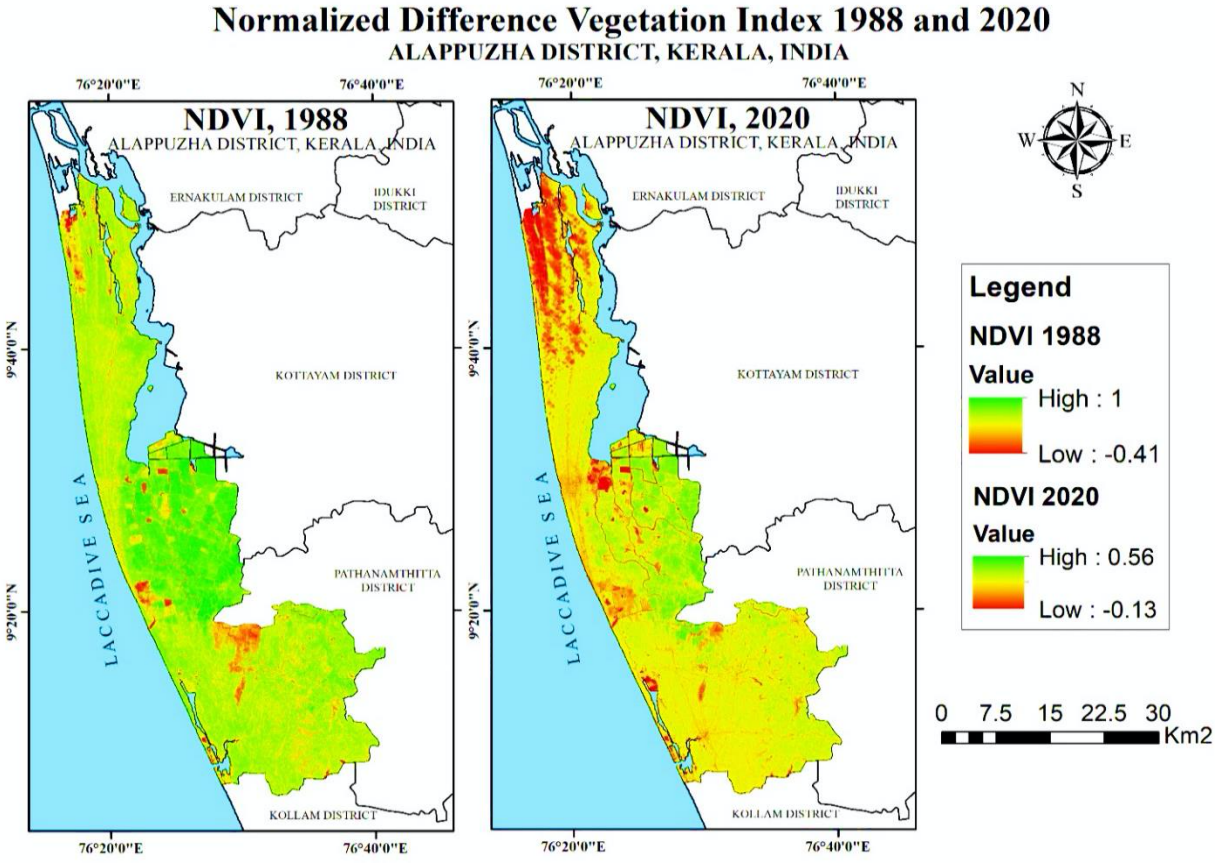

Figure 3b. Spatial distribution of NDVI range of Alappuzha from 1988 to 2020

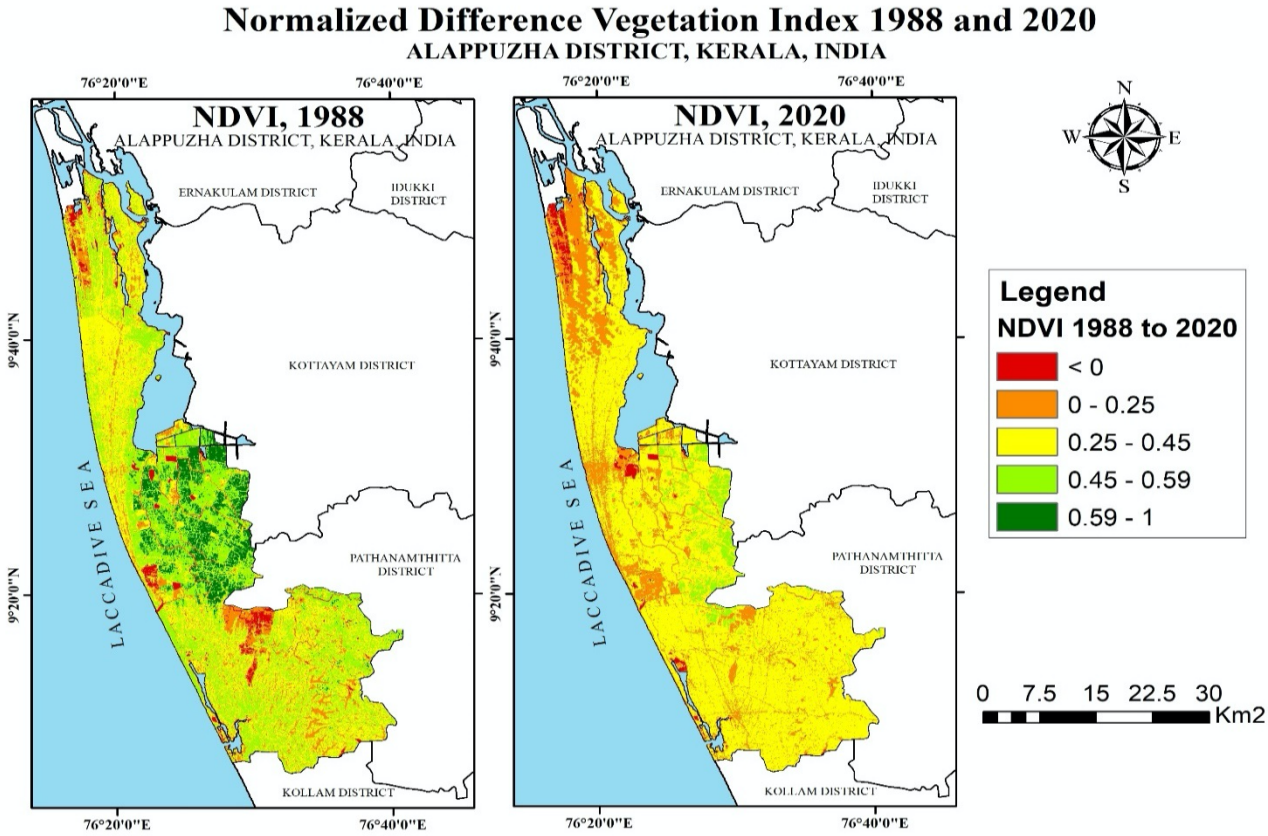

Figure 3c. Spatial distribution of NDVI classes of Alappuzha from 1988 to 2020

Table 3. Spatial distribution of NDVI classes of Alappuzha from 1988 to 2020.

NDVI (ºC) Categories	NDVI Classes	Area Km² (Area in %)		% Difference (1988 to 2020)
		1988	2020	
< 0	No Vegetation	41.86 (3.36)	25.60 (2.06)	-38.85
0 – 0.25	Very low	150.13 (12.06)	277.31 (22.27)	84.71
0.26 – 0.45	Sparse	508.09 (40.81)	885.46 (71.12)	74.27
0.46 – 0.59	Moderate	442.01 (35.50)	56.74 (4.56)	-87.16
>0.6	Highly dense	103.02 (8.27)	0 (0)	-100

3.3 Analysis of SUHI

The spatial distribution of SUHI for the years 1988 to 2020 is depicted in **Figure 4a** and **Table 4**. The analysis of SUHI-affected areas, categorized into six classes, reveals that from 1988 to 2020, the area under the None, weak, and strongest categories, which were 279.33 km², 322.94 km², and 30.22 km² respectively in 1988, decreased to 26.54 km², 181.62 km², and 23.23 km² in 2020, representing a decline of 90.50%, 43.76%, and 23.16% respectively.

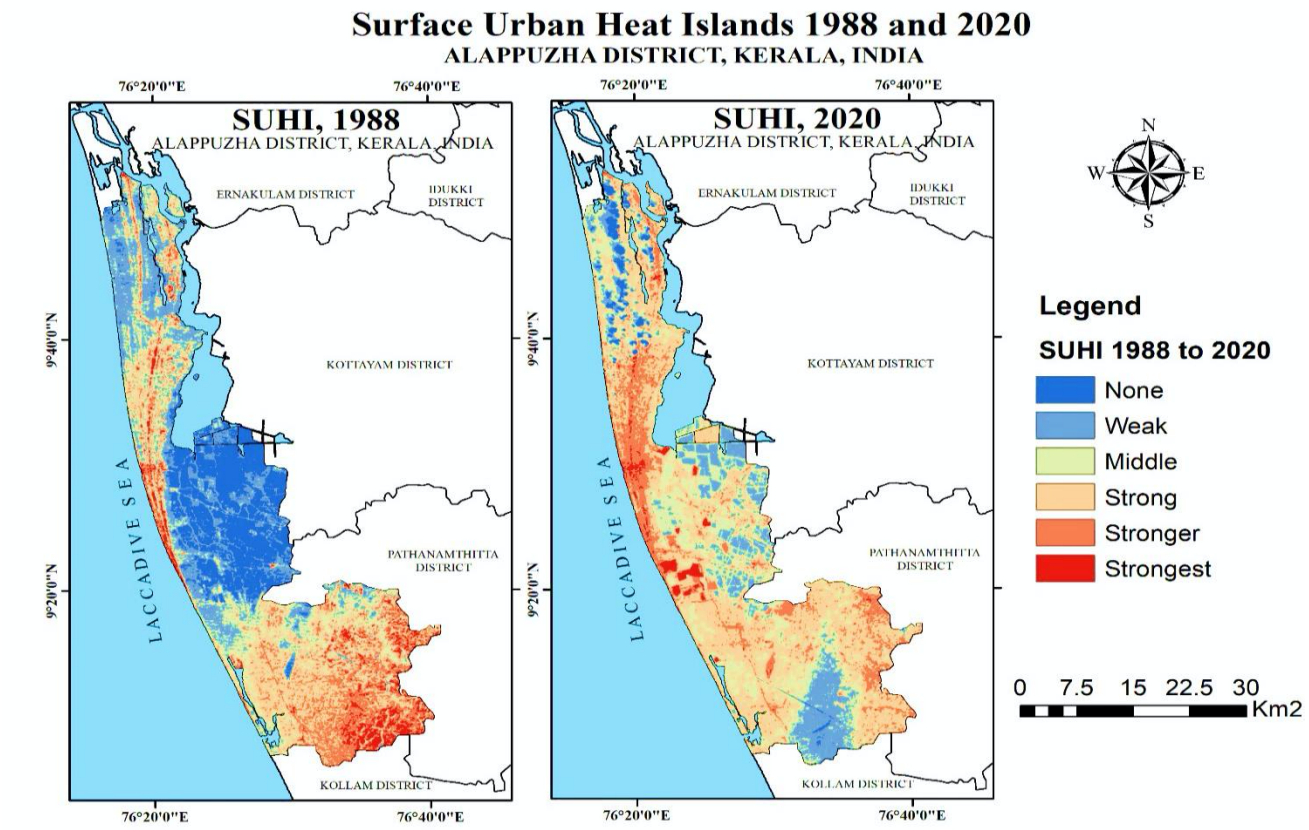

Figure 4a. Spatial distribution of SUHI classes of Alappuzha from 1988 to 2020

Conversely, the area under the middle, strong, and stronger categories, which were 287.98 km², 203.17 km², and 121.46 km² respectively in 1988, increased to 369.89 km², 464.47 km² and 179.35 km² respectively in 2020, showing a growth of 28.44%, 128.62%, and 47.66% respectively, suggestive of a good rate of development in the area. Urbanization of the area, along with loss of vegetation cover and its density, leads to increase in LST, which in turn contributed to the expansion of SUHI areas.

Table 4. Spatial distribution of SUHI classes of Alappuzha from 1988 to 2020

SUHI (°C) Categories	Area Km² (Area in %)		% Difference (1988 to 2020)
	1988	2020	
None	279.33 (22.43)	26.54 (2.13)	-90.50
Weak	322.94 (25.94)	181.62 (14.59)	-43.76
Middle	287.98 (23.13)	369.89 (29.71)	28.44
Strong	203.17 (16.32)	464.47 (37.30)	128.62
Stronger	121.46 (9.79)	179.35 (14.40)	47.66
Strongest	30.22 (2.43)	23.23 (1.87)	-23.16

3.4 Correlation between LST-NDVI

LST and NDVI are highly responsive to environmental changes, with shifts in NDVI potentially leading to alterations in LST, and vice versa. **Figure 5a and b** illustrates a negative correlation between NDVI-LST for the years 1988 and 2020, with R^2 values of -0.4874 and -0.4097, respectively. This suggests that areas with dense vegetation experienced lower surface temperatures, while regions with sparse or inactive vegetation exhibited higher surface temperatures.

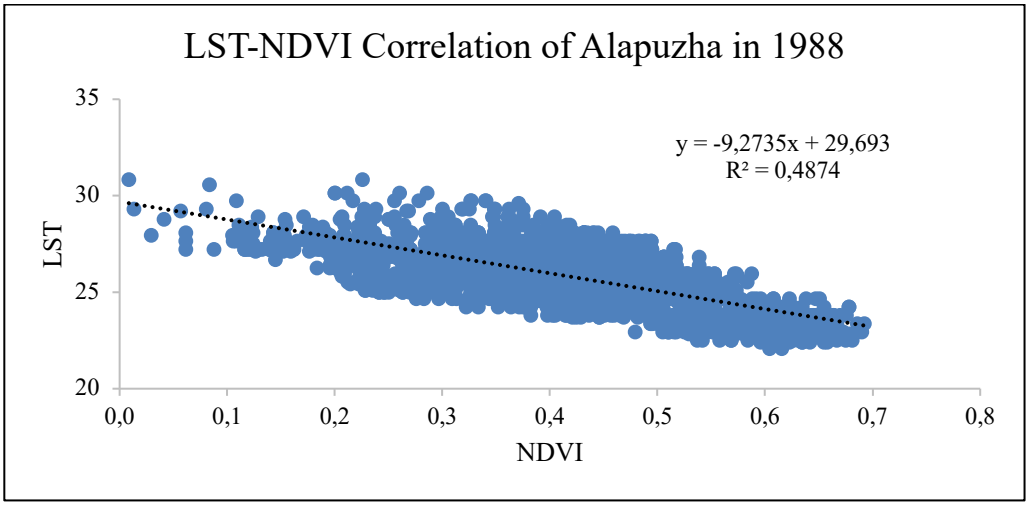

Figure 5a. LST-NDVI Correlation in 1988

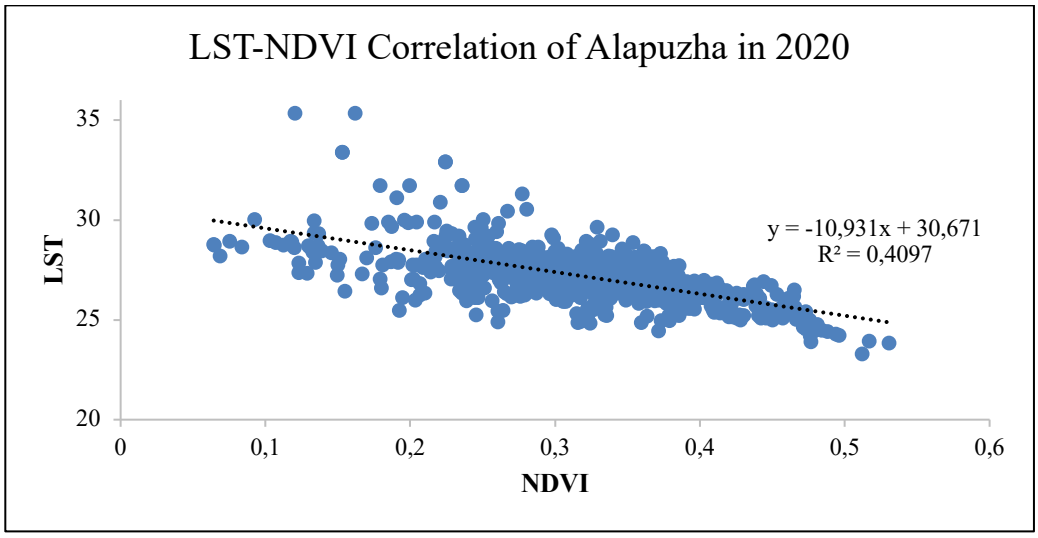

Figure 5b. LST-NDVI Correlation in 2020

Dense vegetation reduces the amount of radiation absorbed by the earth's surface, leading to cooler temperatures. This inverse relationship between LST-NDVI has been documented by numerous researchers for various study regions such as Kottayam (Anitha *et al.*, 2023), Calicut (Chaithanya *et al.*, 2017), Trivandrum, Ernakulam and Kozhikode (Veettil and Grongona, 2018).

Conclusion

The result of the present study reveals that Alappuzha's land uses have been altered significantly. Increase in LST associated with LULC changes has triggered the SUHI phenomenon, with LST sharing an inverse relationship with NDVI. Alappuzha's rising temperatures, driven by urban

expansion from population growth, economic development, and tourism, have intensified SUHI by increasing built-up areas, reducing vegetation, and altering the local energy balance. These changes could lead to adverse health, socio-economic, and ecological effects. Monitoring SUHI in relation to LST and vegetation indices can guide urban planners and policymakers in promoting ecological stability and improving the quality of life. The study recommends increasing urban green spaces to mitigate the UHI effect.

Acknowledgement: The authors thank the Department of Environmental Sciences, Bharathiar University, Coimbatore, Tamil Nadu -641046, for their encouragement and the facilities provided.
Disclosure statement: *Conflict of Interest:* There are no conflicts of interest.
Compliance with Ethical Standards: This article does not contain any studies involving human or animal subjects.

References

Aggarwal S., and Misra, M. (2018, October). Comparison of NDVI, NDBI as indicators of surface heat island effects for Bangalore and New Delhi: Case Study. In *Remote Sensing Technologies and Applications in Urban Environments III* (Vol. 10793, pp. 178-186). SPIE. https://doi.org/10.1117/12.2325738

Amirtham L. R., Devadas M. D., and Perumal, M. (2009). Mapping of micro-urban heat islands and land cover changes: a case in Chennai City, India. *The International Journal of Climate Change: Impacts and Responses*, *1*(2), 71.

Anitha V., Devi M. P., and Prabha D (2023). Bi-Temporal Analysis of Vegetation Index on Land Surface Temperature in Kottayam, Kerala. *Current World Environment,* Vol. 18, No. (3) Pg. 1065-1083 http://dx.doi.org/10.12944/CWE.18.3.13

Artis D. A., and Carnahan, W. H. (1982). Survey of emissivity variability in thermography of urban areas. *Remote sensing of Environment*, *12*(4), 313-329. https://doi.org/10.1016/ 0034-4257(82)900438

Barsi J. A., Schott J. R., Hook S. J., Raqueno N. G., Markham B. L., and Radocinski R. G. (2014). Landsat-8 thermal infrared sensor (TIRS) vicarious radiometric calibration. *Remote Sensing*, *6*(11), 11607-11626. https://doi.org/10.3390/rs61111607

Bora R., and Bora A. K. (2023). NDVI and NDMI indices based land use and land cover change analysis of Charaideu District, Assam, India. *Sustainability, Agri, Food and Environmental Research*, *11*. https://doi.org/10.7770/safer-V11N1-art2726

Carpio M., González Á., González M., and Verichev K. (2020). Influence of pavements on the urban heat island phenomenon: A scientific evolution analysis. *Energy and Buildings*, *226*, 110379. https://doi.org/10.1016/j.enbuild.2020.110379

Chaithanya V. V., Binoy B. V., and Vinod T. R. (2017). Estimation of the Relationship between urban vegetation and land surface temperature of Calicut City and suburbs, kerala, India using GIS and Remote Sensing data. *Int J Adv remote sens*, *6*, 2088-96. DOI: https://doi.org/10.23953/cloud.ijarsg.112

Chander G., and Markham B. (2003). Revised Landsat-5 TM radiometric calibration procedures and postcalibration dynamic ranges. *IEEE Transactions on geoscience and remote sensing*, *41*(11), 2674-2677. https://doi.org/10.1109/TGRS.2003.818464

Chandra S., Sharma D., and Dubey S. K. (2018). Linkage of urban expansion and land surface temperature using geospatial techniques for Jaipur City, India. *Arabian Journal of Geosciences*, *11*, 1-12. https://doi.org/10.1007/s12517-017-3357-6

Chkird F., Azougay A., Mzabri I., Amar I., A Boukroute, A Berrichi, et al. (2024). Provision of urban green spaces: A case study of Oujda City, Northeast Morocco, *Caspian Journal of Environmental Sciences,* 1-19, https://doi.org/10.22124/cjes.2024.7783

Dissanayake D. M. S. L. B., Morimoto T., Ranagalage M., and Murayama Y. (2019). Land-use/land-cover changes and their impact on surface urban heat islands: Case study of Kandy City, Sri Lanka. *Climate*, *7*(8), 99. https://doi.org/10.3390/cli7080099

Dutta D., Rahman A., Paul S. K., and Kundu A. (2021). Impervious surface growth and its inter-relationship with vegetation cover and land surface temperature in peri-urban areas of Delhi. *Urban Climate*, *37*, 100799. https://doi.org/10.1016/j.uclim.2021.100799

Emran A., Roy S., Bagmar M. S. H., and Mitra C. (2018). Assessing topographic controls on vegetation characteristics in Chittagong Hill Tracts (CHT) from remotely sensed data. *Remote Sensing Applications: Society and Environment*, *11*, 198-208. https://doi.org/10.1016/j.rsase.2018.07.005

Faqe Ibrahim G. R. (2017). Urban land use land cover changes and their effect on land surface temperature: Case study using Dohuk City in the Kurdistan Region of Iraq. *Climate*, *5*(1), 13. https://doi.org/10.3390/cli5010013

Gohain K. J., Mohammad P., and Goswami A. (2021). Assessing the impact of land use land cover changes on land surface temperature over Pune city, India. *Quaternary International*, *575*, 259-269. https://doi.org/10.1016/j.quaint.2020.04.052

Grover A., and Singh R. B. (2015). Analysis of urban heat island (UHI) in relation to normalized difference vegetation index (NDVI): A comparative study of Delhi and Mumbai. *Environments*, *2*(2), 125-138. https://doi.org/10.3390/environments 2020125

Guha S., Govil H., Taloor A. K., Gill N., and Dey A. (2022). Land surface temperature and spectral indices: A seasonal study of Raipur City. *Geodesy and Geodynamics*, *13*(1), 72-82. https://doi.org/10.1016/j.geog.2021.05.002

Guo L., Liu R., Men C., Wang Q., Miao Y., and Zhang Y. (2019). Quantifying and simulating landscape composition and pattern impacts on land surface temperature: A decadal study of the rapidly urbanizing city of Beijing, China. *Science of the Total Environment*, *654*, 430-440. https://doi.org/10.1016/j.scitotenv.2018.11.108

Hussain S., Mubeen M., Ahmad A., Majeed H., Qaisrani S. A., Hammad H. M., and Nasim W. (2023). Assessment of land use/land cover changes and its effect on land surface temperature using remote sensing techniques in Southern Punjab, Pakistan. *Environmental Science and Pollution Research*, *30*(44), 99202-99218. https://doi.org/10.1007/s11356-022-21650-8

Jose M., and Padmanabhan M. (2016). Dynamics of agricultural land use change in Kerala: a policy and social-ecological perspective. *International Journal of Agricultural Sustainability*, *14*(3), 307-324. https://doi.org/10.1080/14735903.2015.1107338

Julien Y., Sobrino J. A., Mattar C., Ruescas A. B., Jimenez-Munoz J. C., Soria G., and Cuenca J. (2011). Temporal analysis of normalized difference vegetation index (NDVI) and land surface temperature (LST) parameters to detect changes in the Iberian land cover between 1981 and 2001. *International Journal of Remote Sensing*, *32*(7), 2057-2068. https://doi.org/10.1080/01431161003762363

Kaplan G., Avdan U., and Avdan Z. Y. (2018). Urban heat island analysis using the landsat 8 satellite data: A case study in Skopje, Macedonia. In *Proceedings* (Vol. 2, No. 7, p. 358). MDPI. https://doi.org/10.3390/ecrs-2-05171

Kuang W., Liu A., Dou Y., Li G., and Lu D. (2019). Examining the impacts of urbanization on surface radiation using Landsat imagery. *GIScience & remote sensing*, *56*(3), 462-484 https://doi.org/10.1080/15481603.2018.1508931

Landsat 5: Landsat 7 (L7) Data Users Handbook. Available online: https://prd-wret.s3-us-west-2.amazonaws.com/assets/palladium/production/atoms/files/LSDS-1927_L7_Data_Users_Handbook-v2.pdf (accessed on 5 December 2019).

Landsat 8: Ihlen, V., & Zanter, K. (2019). Landsat 8 data users handbook. *US Geological Survey: Sioux Falls, SD, USA*, *55*.

Leal Filho W., Mandel M., Al-Amin A. Q., Feher A., and Chiappetta Jabbour C. J. (2017). An assessment of the causes and consequences of agricultural land abandonment in Europe. *International Journal of*

Sustainable Development & World Ecology, *24*(6), 554-560. https://doi.org/10.1080/13504509.2016.1240113

Lo C. P., and Quattrochi D. A. (2003). Land-use and land-cover change, urban heat island phenomenon, and health implications. *Photogrammetric Engineering & Remote Sensing*, *69*(9), 1053-1063. https://doi.org/10.14358/PERS.69.9.1053

Mallick J., Kant Y., and Bharath B. D. (2008). Estimation of land surface temperature over Delhi using Landsat-7 ETM+. *J. Ind. Geophys. Union*, *12*(3), 131-140.

Mathew A., Khandelwal S., and Kaul N. (2017). Investigating spatial and seasonal variations of urban heat island effect over Jaipur city and its relationship with vegetation, urbanization and elevation parameters. *Sustainable cities and society*, *35*, 157-177. https://doi.org/10.1016/j.scs.2017.07.013

Mathew A., Sarwesh P., and Khandelwal S. (2022). Investigating the contrast diurnal relationship of land surface temperatures with various surface parameters represent vegetation, soil, water, and urbanization over Ahmedabad city in India. *Energy Nexus*, *5*, 100044. https://doi.org/10.1016/j.nexus.2022.100044

Mathew J. C., and Varghese A. (2022). Impact of urbanization and spatio-temporal estimation of land surface temperature in a fast-growing coastal Town in Kerala, Western Coast of Peninsular India. *Remote Sensing in Earth Systems Sciences*, *5*(4), 207-229. https://doi.org/10.1007/s41976-022-00075-4

Mbow C., Rosenzweig C., Barioni L. G., Benton T. G., Herrero M., Krishnapillai M., and Waha K. (2019). IPCC special report on climate change, desertification, land degradation, sustainable land management, food security, and greenhouse gas fluxes in terrestrial ecosystems. *World Health Organiza-tion and United Nations, Rome*.

Mohammed Firoz C., Banerji H., and Sen J. (2014). A Methodology to Define the Typology of Rural Urban Continuum Settelments in Kerala. *Journal of Regional development and Planning*, *3*(1), 49.

Plieninger T., Hui C., Gaertner M., and Huntsinger L. (2014). The impact of land abandonment on species richness and abundance in the Mediterranean Basin: a meta-analysis. *PloS one*, *9*(5), e98355. https://doi.org/10.1371/journal.pone.0098355 Subedi, Y. R., Kristiansen, P., Cacho, O., & Ojha, R. B. (2021). Agricultural land abandonment in the hill agro-ecological region of Nepal: Analysis of extent, drivers and impact of change. *Environmental Management*, *67*, 1100-1118. https://doi.org/10.1007/s00267-021-01461-2

Prasad G., and Ramesh M. V. (2019). Spatio-temporal analysis of land use/land cover changes in an ecologically fragile area—Alappuzha District, Southern Kerala, India. *Natural Resources Research*, *28*, 31-42. https://doi.org/10.1007/s11053-018-9419-y

Radhakrishnan S., and Geetha P. (2022). Urban sprawl assessment using remote sensing and gis techniques: A case study of ernakulam district. In *Intelligent Sustainable Systems: Selected Papers of WorldS4 2021, Volume 2* (pp. 293-307). Springer Singapore. https://doi.org/10.1007/978-981-16-6369-7 26

Santhosh L. G., and Shilpa D. N. (2023). Assessment of LULC change dynamics and its relationship with LST and spectral indices in a rural area of Bengaluru district, Karnataka India. *Remote Sensing Applications: Society and Environment*, *29*, 100886. https://doi.org/10.1016/j.rsase.2022.100886

Sharma V. P. (2015). Dynamics of land use competition in India: Perceptions and realities.

Siddique M. A., Dongyun L., Li P., Rasool U., Khan T. U., Farooqi T. J. A., and Rasool M. A. (2020). Assessment and simulation of land use and land cover change impacts on the land surface temperature of Chaoyang District in Beijing, China. *PeerJ*, *8*, e9115. doi.org/10.7717/peerj.9115

Snyder W. C., Wan Z., Zhang Y., and Feng Y. Z. (1998). Classification-based emissivity for land surface temperature measurement from space. *International Journal of Remote Sensing*, *19*(14), 2753-2774. https://doi.org/10.1080/014311698214497

Sreya B., and Vidhyavathi A. (2018). Dynamics of land use pattern in Kerala–a temporal analysis. *Madras Agricultural Journal*, *105*(march (1-3), 1.

Streutker D. R. (2003). Satellite-measured growth of the urban heat island of Houston, Texas. *Remote*

sensing of Environment, *85*(3), 282-289. https://doi.org/10.1016 /S0034-4257(03)00007-5

Tesfamariam S., Govindu V., and Uncha A. (2023). Spatio-temporal analysis of urban heat island (UHI) and its effect on urban ecology: The case of Mekelle city, Northern Ethiopia. *Heliyon*, *9*(2). https://doi.org/10.1016/j.heliyon.2023.e13098

Townshend J. R., and Justice C. O. (1986). Analysis of the dynamics of African vegetation using the normalized difference vegetation index. *International Journal of remote sensing*, *7*(11), 1435-1445. https://doi.org/10.1080/01431168608948946

Tucker C. J. (1979). Red and photographic infrared linear combinations for monitoring vegetation. *Remote sensing of Environment*, *8*(2), 127-150. https://doi.org/10.1016/0034-4257(79)90013-0

Ullah N., Siddique M. A., Ding M., Grigoryan S., Zhang T., and Hu Y. (2022). Spatiotemporal impact of urbanization on urban heat island and urban thermal field variance index of Tianjin City, China. *Buildings*, *12*(4), 399. https://doi.org/10.3390/buildings 12040399

Vasanthawada S. R. S., Puppala H., and Prasad P. R. C. (2023) Assessing impact of land-use changes on land surface temperature and modelling future scenarios of Surat, India. *International Journal of Environmental Science and Technology*, 20(7), 7657-7670. https://doi.org/10.1007/s13762-022-04385-4

Veettil B. K., and Grondona A. E. B. (2018). Vegetation changes and formation of small-scale urban heat islands in three populated districts of Kerala State, India. *Acta Geophysica*, *66*, 1063-1072. https://doi.org/10.1007/s11600-018-0189-z

Viswanathan P. K. (2014). The rationalization of agriculture in Kerala: Implications for the natural environment, agro-ecosystems and livelihoods. *Agrarian South: Journal of Political Economy*, *3*(1), 63-107. https://doi.org/10.1177/22779760145302

Weng Q., Lu D., and Schubring J. (2004). Estimation of land surface temperature–vegetation abundance relationship for urban heat island studies. *Remote sensing of Environment*, *89*(4), 467-483. https://doi.org/10.1016/j.rse.2003.11.005

Xiong Y., Huang S., Chen F., Ye H., Wang C., and Zhu C. (2012). The impacts of rapid urbanization on the thermal environment: A remote sensing study of Guangzhou, South China. *Remote sensing*, *4*(7), 2033-2056. https://doi.org/10.3390/rs4072033

Zhang Y., Yiyun C., Qing D., and Jiang P. (2012). Study on urban heat island effect based on normalized difference vegetated index: a case study of Wuhan City. *Procedia environmental sciences*, *13*, 574-581. https://doi.org/10.1016/j.proenv.2012.01.048

Zhou B., Rybski D., and Kropp, J. P. (2013). On the statistics of urban heat island intensity. *Geophysical research letters*, *40*(20), 5486-5491. https://doi.org/10.1 002/2013GL057320